The Modeling of Trapped-Fetch Waves with Tropical Cyclones—A Desktop Operational Model

ALLAN W. MACAFEE

National Laboratory for Marine and Coastal Meteorology, Meteorological Service of Canada, Dartmouth, Nova Scotia, Canada

PETER J. BOWYER

Canadian Hurricane Centre, Meteorological Service of Canada, Dartmouth, Nova Scotia, Canada

(Manuscript received 6 February 2004, in final form 29 November 2004)

ABSTRACT

The authors' development of an underlying theory of trapped-fetch waves with tropical cyclones was presented in an earlier paper. Based on this work a simple, desktop Lagrangian-based trapped-fetch wave model was developed. Although initially a training tool, operational meteorologists recognized that the model could assist them in real-time assessment of trapped-fetch wave potential. Hence, the model was integrated into the Canadian Hurricane Centre's operational prediction workstation. Because of this integration and the computational speed of the model, after reviewing the output from a full spectral wave model, the forecaster uses this simple model to assess, in more detail, trapped-fetch wave potential in various track prediction scenarios.

The trapped-fetch wave model and the ensemble of parametric hurricane wind models used to drive the model are outlined in this paper. A number of case studies are examined and additional applications suggested.

1. Introduction

Tropical cyclones (TCs) are among the most difficult phenomena in the atmosphere to fully describe and predict and engineers and scientists often resort to parameterized winds (Phadke et al. 2003). Bowyer and MacAfee (2005) have shown the importance and sensitivity of wind speed, storm speed, and fetch length, in the development of large trapped-fetch waves (TFWs), especially near those critical storm speeds at which moving storms generate the highest waves.

The authors have developed a Lagrangian TFW model for use in training operational meteorologists and as a TFW-potential assessment tool used by the forecasters at the Canadian Hurricane Centre (CHC). This model was first used operationally in 2000 (MacAfee and Peters 1999; MacAfee and Bowyer 2000b) and has been recently refined through improved parameterization, both with respect to wave generation and wind modeling. The model deals specifically with wind-driven wave growth in trapped-fetch situations in the TC environment. Since it employs the assumption that dominant TFWs have one spectral mode (Bowyer and MacAfee 2005), the development of a unimodal spectrum is possible using basic wave growth equations. The model has been developed to answer three questions that forecasters often have when forecasting waves with TCs: Where, when, and how big, will the biggest waves be? The model does not predict wave height fields or spectral fields; it is intentionally focused on predicting maximum possible wave heights with a TC.

Full spectral wave models have the capability to capture the details of TC wave systems exhibiting a high degree of wave containment (Bowyer and MacAfee 2005). However, their most significant operational limitation is their inability to allow last-minute storm changes in order to generate new wind and wave model solutions and meet forecasting time constraints. As well, the more sophisticated models do not allow for different real-time scenarios (or ensembles) to be run at forecasters' discretion. This limitation can be significant when forecasting parameters associated with TCs because of the often-erratic nature of their track. Therefore, it is essential for forecasters to be able to update TFW trajectories in order to assess storm parameter sensitivities, especially for storms predicted to move near their critical speed. The TFW model focuses on a single, specific aspect of the wave field: the highest po-

Corresponding author address: Allan W. MacAfee, National Laboratory for Marine and Coastal Meteorology, Meteorological Service of Canada, 45 Alderney Dr., Dartmouth, NS B2Y 2N6, Canada.
E-mail: al.macafee@ec.gc.ca

tential waves due to wave containment. Hence, the model output must always be used only after first reviewing the full spectral wave model output, which provides a picture of the overall wave field.

Computer limitations and timeliness of output dictate that compromises be made when building an operational forecasting tool. As a result, the CHC TFW model was intentionally designed to run on a forecaster workstation (Linux platform) with output available in a measure of seconds. For example, to model the TC-centered wind fields and compute the TFWs for the longest TC trajectory in the history of the Atlantic (702 h during Hurricane Ginger in 1971) takes 51 s. Because the model has been fully integrated into the forecaster's working environment, as the forecaster graphically draws a predicted track, adjusts intensity, and position, or motion, the parametric hurricane wind models and the TFW model automatically record and respond to the updated information and reassess the TFW potential. Hence, with minimal effort, a variety of scenarios can be run to supply the forecaster with a measure of confidence in their prediction.

Because of the computational speed of the model, TFW potential for the full track of a TC can be recomputed after the latest predicted track segment is automatically merged with the historical portion. Hence, potential TFW impacts other than along the predicted track can be noted.

Following from the operational perspective on the theory of TFW with TCs (Bowyer and MacAfee 2005), this paper outlines an operational tool for deep-water wave forecasts of the height, location, and arrival time of the largest waves. In section 2, four operational parametric wind models, which drive the TFW model, are reviewed. Section 3 describes the TFW model, section 4 presents case studies, section 5 highlights operational utility, and section 6 provides conclusions.

2. Wind models

The wind field input into the TFW model can be analysis generated or model generated. In this paper, the focus is on a model-generated wind field. Such a wind field must accurately depict the 2D structure of a TC while allowing for real-time modification through forecaster intervention as the storm evolves. The former criterion was met by using an ensemble of well-documented parametric hurricane wind models. The latter criterion was satisfied by integrating the wind model into the CHC forecasting workstation, thus using predicted modeling parameters defined and modified during the track creation process. In all the model equations described below, V_m is the maximum wind (m s^{-1}), R is the radial distance to the grid point (km), and R_m is the radius of maximum winds (km).

The modified Rankine vortex model was described in Phadke et al. (2003). The model equations are

$$V = \begin{cases} V_m\left(\dfrac{R}{R_m}\right)^B, & R < R_m \\ V_m\left(\dfrac{R_m}{R}\right)^B, & R \geq R_m \end{cases}; \tag{1}$$

B is a shape factor set at 0.5 as suggested by Phadke et al. (2003).

The Sea, Lake, and Overland Surges from Hurricanes (SLOSH) wind model was described by Houston and Powell (1994) and validated against the Hurricane Research Division's (HRD) H*WIND analysis by Houston et al. (1999). The model equation is

$$V = V_m \frac{2RR_m}{(R_m^2 + R^2)}. \tag{2}$$

The Holland wind model was described in Holland (1980). The model equations are

$$V = \left\{\left(\frac{R_m}{R}\right)^B \frac{B(P_n - P_c)}{\rho} \exp\left[-\left(\frac{R_m}{R}\right)^B\right] + \frac{R^2 f^2}{4}\right\}^{(1/2)} - \frac{Rf}{2}$$
$$B = e\rho \frac{V_m^2}{(P_n - P_c)}, \tag{3}$$

where $f = 2\ \Omega\ \sin\phi$ is the Coriolis parameter, ρ is air density, e is 2.71828, B is the shape parameter, P_c is the central pressure, and P_n is the sea level pressure at the last closed isobar around the TC.

A vortex simulation model was described in DeMaria et al. (1992). The model equation is

$$V = V_m\left(\frac{R}{R_m}\right) \exp\left\{\frac{1}{B}\left[1 - \left(\frac{R}{R_m}\right)^B\right]\right\}; \tag{4}$$

B is a shape parameter determined using the mean position of a specific wind contour (beyond R_m), for a given strength TC. This constraint was given by

$$\left(\frac{R_c}{R_m}\right)^B + B\ \ell n\left(\frac{V_a R_m}{R_c V_m}\right) - 1 = 0$$
$$V_a = \frac{-X_1 \pm (X_1^2 - 4X_2^2)^{1/2}}{2}$$
$$X_1 = 2\sin\theta_R \frac{V_{\rm st} R_m R_c}{(R_m^2 + R_c^2)}$$
$$X_2 = \left[\frac{V_{\rm st} R_m R_c}{(R_m^2 + R_c^2)}\right]^2 - V_c^2, \tag{5}$$

where $V_{\rm st}$ is the storm speed, θ_R is the angle of the grid point relative to $V_{\rm st}$, V_a is the nontranslational speed-adjusted wind, and R_c is the distance to the critical wind speed V_c, in this study, 17 m s^{-1} (34 kt).

The TC translational adjustment at each model grid point was computed by resolving the tangential wind into storm-relative U and V components then adding a radially weighted storm speed (Phadke et al. 2003) to the y component:

$$U = -V_a \cos\theta_R$$
$$V = V_a \sin\theta_R + \left(\frac{V_{\rm st}R_m R}{(R_m^2 + R^2)}\right)$$
$$V_{\rm GPT} = (U^2 + V^2)^{(1/2)}, \qquad (6)$$

where $V_{\rm GPT}$ is the motion-adjusted wind speed. Equation (6) was applied to all parametric models except Holland where the radially-weighted storm speed term was set to zero, which is more appropriate for an equation based on gradient wind theory.

Following Holland (1980), an MSL pressure grid was computed using

$$P = P_c + (P_n - P_c)\exp\left[-\left(\frac{R_m}{R}\right)^B\right]$$
$$B = e\rho\frac{V_m^2}{(P_n - P_c)}, \qquad (7)$$

where ρ is the air density (1.15 kg m^{-3}). Finite differencing was used to compute the geostrophic wind direction of a unit vector at each grid point. A cross-isobaric flow correction (β) was applied using the scheme outlined in Phadke et al. (2003):

$$\beta = \begin{cases} 10^\circ + \left(1 + \dfrac{R}{R_m}\right), & R < R_m \\ 25^\circ + \left(\dfrac{R}{R_m} - 1\right), & R_m \le R < 1.2R_m \\ 25^\circ, R \ge 1.2R_m \end{cases}. \qquad (8)$$

The parametric models are based on gradient wind theory and data collected from aircraft at flight levels from 925 to 700 hPa. All computed winds were adjusted to the 10-m level using a model-specific factor from 0.86 to 0.89 based on Franklin et al. (2003) and comparisons with HRD wind analyses. To match the time step of the TFW model, the wind is converted from 10 min to 1 h using a gust factor of 0.92 (Krayer and Marshall 1992). The model-generated wind fields were not adjusted to include wind reduction due to overland flow.

For a given TC track location (hereafter TL), each parametric model requires V_m, P_c, $\mathbf{V}_{\rm st}$, and R_m. In addition, the Holland model requires P_n and the vortex model requires R_{34}. For case studies of historical TCs, V_m and P_c are obtained from the National Hurricane Center's hurricane database archive (HURDAT). For real-time application, V_m and P_c are available from the CHC workstation, which records analysis of past positions and the forecaster-generated predicted track.

The value of P_n is extracted from a table of average monthly values for the Gulf of Mexico and four subbasins in the Atlantic (<25°N, 25°–35°N, 35°–45°N, >45°N). To address TC asymmetries, R_m and R_{34} are extracted from tables created by analyzing HRD gridded wind fields (H*WIND) from 1998 to 2003. From each H*WIND analysis, R_m was extracted from 16 storm-relative radial profiles and sorted by the storm maximum wind into categories (horizontal axis of Fig. 1). A normal distribution was applied to the random sample in each category to remove outliers (±1.5 std dev). Vickery et al. (2000) gives an equation for the variation of R_m with latitude [Eq. (7)] but indicates that north of 30°N the model is inaccurate. Since the focus of this paper is on rapidly moving TCs—in particular, those north of 30°N—a statistical weighting function for TC motion derived from the HRD dataset is applied to the independently computed, latitude-dependent value, to inflate (deflate) R_m at high (low) latitudes. In the model, each grid point's radial angle was computed, then R_m was determined at adjacent radial profiles and interpolated to that grid point. A similar method (not shown) was used to generate R_{34}.

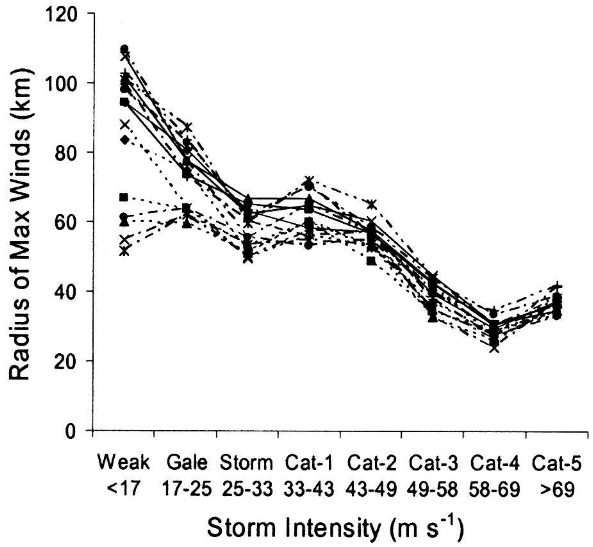

FIG. 1. Radius of maximum wind (R_m) curves, extracted along radial profiles from the storm center at 22.5° intervals, for different classes of storm intensity. (Storm data: HRD gridded winds for 389 storms from 1998 to 2003.)

For a real-time TC, parameters are automatically defined and updated as the forecaster graphically constructs (edits) a predicted track, which is the cornerstone of the CHC prediction system. Because of the computation speed of the wind model [the 702 wind grids of Ginger in 1971 in 4 s], wind grids are recomputed as track and intensity changes are made. Because the TFW model requires wind grids for the entire track, the latest predicted track is appended automatically to the historical track prior to modeling. Any reanalysis of historical information will be reflected in the updated model run.

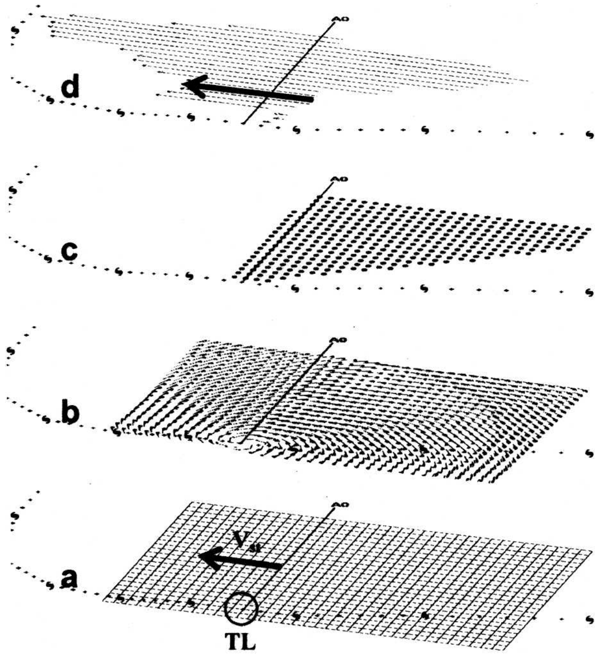

FIG. 2. Schematic diagram showing the successive steps in defining initial wave calculation points at a track location (circled and labeled TL): (a) construct a model grid right of track, oriented parallel to the storm motion $\mathbf{V}_{st}$ (heavy arrow) and locate the reference line A_0, (b) create a wind field using a parametric model, and (c) apply criteria to select initial wave calculation points. The TFW model output for the selected points is displayed as trajectories in (d); the dominant trajectory for the TL is denoted by a heavier arrow.

The use of statistical estimates of some model parameters (i.e., R_m) in lieu of observed values from aircraft, satellite, or surface observations is a justifiable limitation; observable data are not always available in real time and may be too labor intensive to incorporate into the duty forecaster's routine. In addition, the model described in this paper was designed to be an assessment tool where relative wave height values and trends are as important as absolute values. As well, using a consistent set of input parameters ensures that variations in the generated wind field are solely due to the design of each parametric model.

Figure 2a shows a typical 37 × 25 grid with 11-km (6 n mi) spacing created at a given track location (TL). The grid is oriented along $\mathbf{V}_{st}$, right of track, and offset. Offsetting the grid provides adequate overlap between consecutive grids, ensures that all potential TFW are modeled (Bowyer and MacAfee 2005), and optimizes computation time. In addition, the grid domain is intentionally small to avoid unrealistic winds at larger distances from the TL recalling that the intent is to delineate the maximum wave trajectories and not generate a complete 2D wave field. Bretschneider and Tamaye (1976) found that the maximum TFW should be in the range 1–2 times R_m, well within the specified grid domain.

3. TFW model

a. Wave equations

The wave equations used in the TFW model are from Bretschneider and Tamaye (1976):

$$\frac{gH_{\mathrm{SIG}}}{U^2} = A_1 \tanh\left[B_1\left(\frac{gF}{U^2}\right)^{m_1}\right]$$
$$\frac{C_o}{U} = \frac{gT_P}{2\pi U} = A_2 \tanh\left[B_2\left(\frac{gF}{U^2}\right)^{m_2}\right]$$
$$t_{\min} = 2\int_0^{F_{\min}} \frac{1}{C_o}\,\mathrm{d}x, \tag{9}$$

where H_{SIG} is the significant wave height (ft), T_P is the significant wave period (s), F is the fetch length (ft), U is the 10-min average surface wind speed at the 10-m level (ft s^{-1}), $t_{\min}$ is the wind duration (s), C_o is the wave speed (ft s^{-1}), and g is the acceleration due to gravity (ft s^{-2}). The coefficients are $A_1 = 0.283$, $A_2 = 1.2$, $B_1 = 0.0125$, $B_2 = 0.077$, $m_1 = 0.42$, and $m_2 = 0.25$.

In these equations, given a wind speed, an initializing fetch length, and a time interval, wave height and period, growth duration, and equivalent fetch, can be computed. Because of the multivariable inputs, the variables are input iteratively into the equations until the limiting variable forces a convergence (arbitrarily 0.1%) to a wave height solution. The computed duration time may be less than the initial estimated wind duration as it is dependent on the wave growth and limited by the time to reach a fully developed sea. The *equivalent fetch* is the distance the waves must travel to achieve wave height H when subjected to a constant wind U. To ensure that the equivalent fetch is not underestimated during the iterative calculations, the input fetch is set at an arbitrarily large value of 2000 n mi (3706 km) to simulate a realistic unlimited fetch condition.

In applying Eq. (9), the fetch-limited nature of the Bretschneider equations implies that fetch width limitations in TCs have not been addressed. The impact of this limitation is discussed in Bowyer and MacAfee (2005).

b. Procedure

The HURDAT 6-hourly or real-time 6- or 12-hourly positions are converted to 1-h TLs using linear interpolation. A modeling grid is constructed at each TL and a wind field computed (Fig. 2b). Following Bowyer and MacAfee (2005), a Lagrangian-based method for calculating TFW is employed. Initial wave calculation points on each TL grid are determined using the winds. A reference line A_o extends right of TL and orthogonal to $\mathbf{V}_{st}$. Each grid row perpendicular to A_o represents a set of points from which trajectories could be computed; however, the winds at points distant from A_o

may not be relevant source points: either the trajectories are not parallel to the track or the wind is of insufficient strength to be considered for TFW. Hence, along each grid row across A_o, the winds forward of A_o are examined and those points satisfying the (wind direction $-$ $\mathbf{V}_{st}$) difference criterion (D_{CRIT}) of $<30°$ are retained (Saville 1954). The strong wind shift ahead of A_o (Fig. 2b) precludes the need for a companion wind speed criteria as D_{CRIT} will always be satisfied first. Similarly, the points trailing A_o are retained if the preceding D_{CRIT} is met and the wind speed at a point is within 75% of the component of the A_o wind along $\mathbf{V}_{st}$. The threshold of 75% was selected following extensive testing: thresholds <75% generate lower TFW of shorter duration; thresholds >75% only marginally increase TFW (<0.25 m) yet add significantly to computation time. Figure 2c illustrates the reduced, noninteracting initial wave point calculation set achieved by applying these criteria.

Consider a grid row across A_o and the initial wave calculation points along that row. At T_0, at each of these points, the local wind speed component along $\mathbf{V}_{st}$, an initializing fetch of 3704 km (2000 n mi) (Bowyer and MacAfee 2005), and the TFW model time step of 1 h are input to the wave growth equations [Eq. (9)] to generate significant wave height (H_{SIG}), significant wave period (T_P), duration, and equivalent fetch values. During the time step, waves from the initial calculation points travel a distance equal to the equivalent fetch along the row. At their new position, these waves are subjected to the local wind field of the next TL (1 h later). Using the wind field as in Fig. 2b and applying bilinear interpolation, the local wind over the waves is determined, and using D_{CRIT}, the new wind direction is tested against $\mathbf{V}_{st}$ at T_0. If D_{CRIT} is not satisfied, the waves are flagged as having reached their TFW limit and are no longer computed. Otherwise, the potential for further growth is assessed by computing the highest fully developed seas H_{FD} (m) using the relationship

$$H_{FD} = \begin{cases} \left(\dfrac{U}{5.8863}\right)^2, & U \leq 10.3\ \mathrm{m\,s^{-1}} \\ \left(\dfrac{U}{0.03040U + 5.5555}\right)^2, & 10.3 < U \leq 23.1\ \mathrm{m\,s^{-1}} \\ \left(\dfrac{U}{0.04685U + 5.1954}\right)^2, & U > 23.1\ \mathrm{m\,s^{-1}} \end{cases} \tag{10}$$

and comparing the result to the current wave height H. If $H \geq H_{FD}$, then the waves have moved into an area where the local winds can no longer support them; hence, they are no longer computed. If $H < H_{FD}$, there is potential for further growth. As long as all criteria are satisfied, the calculations are repeated through successive time steps. With each successive iteration, as criteria are no longer met, the number of wave calculation points decreases until there are no remaining points in a row. The highest waves for that row are recorded as a trajectory as shown in Fig. 2d. In turn, each row for a given TL is processed before proceeding to the next initiating TL where another independent set of initial wave calculation points seed a new set of iterations.

Wave calculation points are noninteractive and the waves generated from an earlier TL do not precondition downstream initial wave calculation points. As well, grids are aligned with the local $\mathbf{V}_{st}$ and cover a limited domain near the TL. As waves move, they may not reach the next grid and, by necessity, computations are terminated; analysis has shown that in most situations these waves have moved toward increasingly weaker wind and are unlikely to experience significant further growth.

The trajectories of Fig. 2d are the set generated for a single TL. Although some predicted wave heights are equal and their trajectories have similar length, the number of hours of growth (not shown) can be significantly different; waves do not arrive in the same area at the same time. Given that additional sets of trajectories are generated hourly along the track, care must be taken in interpreting the model output. Because of this complexity, model output displays the trajectory, which represents the dominant TFW: the highest waves in the set of trajectories for each TL. In Fig. 2d, the heavy arrow indicates this dominant TFW.

c. *Context*

A full spectral wave model provides a complete prediction of the wave field including the spectral mode simulated by the TFW model; however, the generating region and timing of arrival of the waves of greatest impact (which may or may not be the highest waves) might be missed during the operational examination of contoured maps at specific synoptic hours. The alternate approach of the TFW model acts as a "drill down" to attempt to extract more information about one particular aspect of the wave field. In turn, the analysis of TFW output should lead the forecaster back to a more in-depth examination of the full spectral wave model output, resulting in an improved forecast product. The TFW model output is not sufficient, nor intended, to provide a complete depiction of a wave field.

The wave equations [Eqs. (9) and (10)] are applicable only for wave development in deep water. The current version of the TFW model does not recognize the transition from deep to shallow water and will continue to apply the equations inappropriately in the coastal zone. Hence, the height of wave trajectories approaching the coastline may be in error. This limitation will be addressed in a future version of the model.

4. Case studies

Four different Atlantic tropical cyclones were chosen for detailed case study investigation of the TFW model

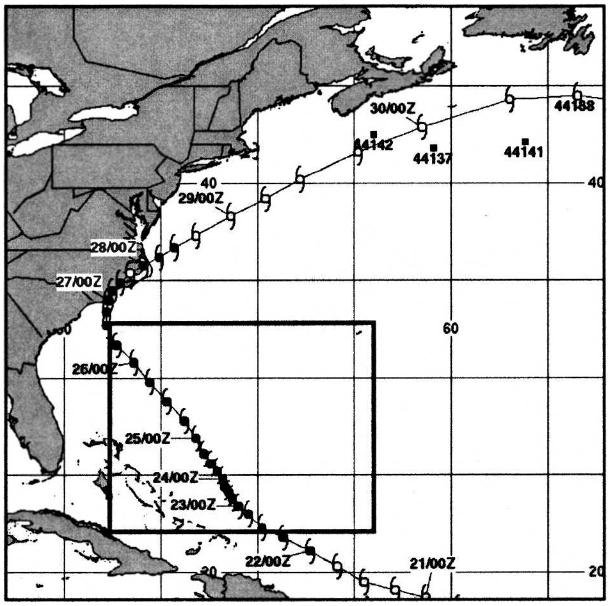

FIG. 3. Track of Bonnie in 1998 with the box indicating the zoomed area used in Fig. 6.

(Bonnie and Danielle in 1998; Luis in 1995; and Juan in 2003) along with five other examples from the Gulf of Mexico. The TFW model was run for each wind model listed in section 2. Results from all TFW model simulations, identified by the driving wind models, will be presented for the first case. Thereafter, for brevity, only the Holland model results will be displayed. Given that the TFW model is unimodal, discussion will be confined to H_{SIG}. In comparing model output to buoy data, no consideration was given to the wave sampling offset times of nearly 40 min (AXYS 1996) except where noted. Accordingly, H_{SIG} are assumed valid at transmission times.

a. Bonnie 1998—North

On 30 August 1998, Bonnie—a 23 m s^{-1} (45 kt) tropical storm—passed approximately 139 km (75 n mi) north-northwest of buoy 44137 (Fig. 3) near the arrival of the wave maximum (Table 1). Eight hours later the maximum H_{SIG} reached buoy 44141 one hour after the nearest approach of Bonnie. Note the sharp boundary in the spectral wave density plot of Fig. 4 at the time of the maximum in the H_{SIG} reports indicating the significant lack of preceding waves: an indication of strong wave containment or resonance (Jones et al. 2003; Bowyer and MacAfee 2005).

Figure 5 shows the TFW model output with the dominant TFW trajectories from each TL. Compare the position and values of the H_{SIG} for the TFW cluster in the circled area: 11 m for models Figs. 5a–c and 10 m for model d; the cluster is moving toward buoy 44137, which reported 10.8 m. The gradually increasing forward speed of Bonnie indicates a system exhibiting strong wave containment (Bowyer and MacAfee 2005) as demonstrated by the length of the trajectories (the effective fetch), some growing for 45 h. As discussed in Bowyer and MacAfee (2005), the left-of-track buoy 44142 should have a lower maximum H_{SIG} (Table 1) than right of track. Note the cluster of 11-m trajectories in Fig. 5a directed across the track toward buoy 44142. These TFWs originated from the TL grid at 1800 UTC 27 August 1998 where the change in direction of Bonnie was quite abrupt and 1 h before the beginning of TFWs directed toward buoy 44137. The cross-track TFWs arriving after the storm passage illustrate the importance of examining the TFW model output along the entire track. Note that the longest TFWs originated when the storm center was at its weakest intensity over land on 27 August 1998 (Fig. 5).

b. Bonnie in 1998—South

Prior to moving into Canadian waters, Bonnie had been a 51 m s^{-1} (100 kt) hurricane moving toward the U.S. east coast (Fig. 3). During this stage in the storm's history, scanning radar altimetry (SRA) data were gathered during a flight through the storm around 2100 UTC 24 August 1998 (Wright et al. 2001), reporting a maximum in the H_{SIG} field of 10.8 m (T_P near 13.0 s)

TABLE 1. Maximum significant wave height (H_{SIG}), maximum wave height (H_{MAX}), and wave period (T_P) reported from buoys during passage of selected tropical cyclones. (Source: Marine and Environmental Data Service: information online at http://www.meds-sdmm.dfo-mpo.gc.ca.)

Tropical cyclone	Buoy identifier	Lat (°N), Lon (°W)	H_{SIG} report time and date (hours to storm arrival)	H_{SIG} (m)	H_{MAX} (m) (hours after H_{SIG} report)	T_P (s)
Luis 1995	44139	44.13, 57.64	0200 UTC 11 Sep (−2)	9.1	20.1 (2)	18.3
	44141	42.07, 56.15	0100 UTC 11 Sep (−1)	17.1	30.2 (0)	18.3
Bonnie 1998	44137	41.83, 60.94	0000 UTC 30 Aug (0)	10.8	15.3 (2)	15.1
	44138	44.26, 53.62	1300 UTC 30 Aug (−1)	7.9	14.4 (2)	12.2
	44141	42.11, 56.18	0800 UTC 30 Aug (−1)	10.5	17.9 (0)	13.5
	44142	42.50, 64.02	2100 UTC 29 Aug (−1)	6.5	10.9 (0)	14.2
Danielle 1998	44137	41.83, 60.94	0600 UTC 03 Sep (−2)	5.9	10.9 (2)	13.5
	44138	44.26, 53.62	1400 UTC 03 Sep (1)	12.0	20.3 (1)	15.1
	44141	42.11, 56.18	0800 UTC 03 Sep (0)	15.8	26.9 (0)	18.3
	44142	42.50, 64.02	1600 UTC 03 Sep (5)	3.3	5.5 (−13)	11.6
Juan 2003	44142	42.50, 64.02	2300 UTC 28 Sep (0)	12.2	26.0 (0)	17.1
	44258	44.54, 63.35	0400 UTC 29 Sep (−1)	9.0	19.9 (0)	12.8

located approximately 160 km (86 n mi) northeast of the storm center. Moon et al. (2003) constructed a model swath of H_{SIG} along the track; the 10- and 14-m H_{SIG} contours are shown in Fig. 6a.

Figure 6a shows the TFW model output in a zoom of the boxed area of Fig. 3. All four models develop trajectories beginning 24 August 1998, which persist for 24–48 h. Bonnie was already showing wave containment by late on 24 August where 90% of the peak spectral density was found in a single spectral mode in the wave containment quadrant (Wright et al. 2001; Moon et al. 2003). The TFW model predicted considerably higher waves in the ensuing 24 h as storm wave containment became more pronounced. All four models developed dominant trajectories slightly farther right of track than was shown by Moon et al. (2003).

In Fig. 6b, detailed trajectories for a single TL (0600 UTC 24 August 1998) are shown for each grid row within the storm. This TL is the starting point for model waves passing closest to the SRA wave maximum near the SRA data time (denoted by the asterisk in Fig. 6b). The inset table in Fig. 6b lists H_{SIG}, T_{SIG}, and duration of wave growth, for each trajectory. Although several trajectories are of nearly equal duration and wave height, the dominant TFW is 9.6 m. The model's dominant waves reached 11 m north of the SRA location. The model T_{SIG} of 12 s relates statistically to a T_P of 14 s (WMO 1998) in comparison to the SRA-measured T_P of 13 s.

Note the shift in location of dominant wave trajectories on 23–24 August 1998 (Fig. 6a). Prior to 0000 UTC 23 August 1998, Bonnie was moving northwest at uniform speed. After 0000 UTC 24 August 1998, Bonnie began accelerating to the north-northwest, resulting in sudden changes in the TFW (Moon et al. 2003).

c. Danielle in 1998

On 3 September 1998, Danielle—a 36 m s^{-1} (70 kt) hurricane—passed approximately 56 km (30 n mi) northwest of buoy 44141 (Fig. 7) near the arrival of the wave maximum (Table 1). Maximum H_{SIG} reported by the buoys to the right of track were much higher than those left of track. Note the sharp boundary in the spectral wave density plot of Fig. 4 and the steepness of the wave growth curve at buoy 44141 just prior to the maximum H_{SIG}. Along with the complete lack of preceding swell, these are both indicators of strong wave containment (Bowyer and MacAfee 2005).

Figure 7 shows the output with the largest H_{SIG} of 21 m directed south of buoy 44141. The four models showed considerable variability in the maximum H_{SIG} value (16–21 m) and location of trajectory end points from 556 to 833 km (300 to 450 n mi) upstream of buoy 44141. All models grew TFWs in excess of 24 h indicating strong wave containment—an expected result considering the gradual increase in the hurricane's forward speed on 1–2 September 1998. TFW wave growth terminates upstream from buoy 44141. Applying a first-order approximation for swell decay of long period waves (15–20 s) over 10 h of 22% (WMO 1998) yields waves of 11–16 m near buoy 44141 in reasonable agreement with the observations (Table 1). As in Bonnie, a 17-m TFW trailing the main cluster is directed across the track toward buoy 44137.

The very high TFWs predicted with Danielle give a better sense of the importance of storm speed than a discussion of theory. For example, compare the model output of Danielle with that of Hurricane Gilbert (in 1988): a much stronger, but more slowly moving storm. Figure 8 shows TFW output when Gilbert was at its peak intensity: the 22-m trajectories north of the Yucatan Peninsula (insert Fig. 8). The TFWs from all four models are nearly identical to those found with Danielle, ranging from 16 to 21 m. Danielle was a 36 m s^{-1} (70 kt) hurricane, accelerating gradually from 5 to 15 m s^{-1} (10 to 30 kt) over a span of 30 h. Gilbert, on the other hand, was an 82 m s^{-1} (160 kt) hurricane weakening to 51 m s^{-1} (100 kt) during the 24 h of wave growth, moving at a constant speed of less than 8 m s^{-1} (15 kt). The comparison of these two storms illustrates the importance of storm speed in wave generation.

d. Luis in 1995

On 10–11 September 1995, Luis—a large 44 m s^{-1} (85 kt) hurricane—passed approximately 222 km (120 n mi) northwest of buoy 44141 (Fig. 9) near the arrival of the wave maximum (Table 1). The *Queen Elizabeth II* (*QE II*) luxury liner (denoted by an X in Fig. 9) reported extremely high maximum waves of 29 m, suggesting similar H_{SIG} values to those at buoy 44141 (wave density spectrum unavailable). Lower maximum H_{SIG} were reported at buoy 44139 in the path of Luis and at buoy 44142 (not shown) well west of the track. Buoy 44137 failed on 1200 UTC 9 September 1995 prior to the arrival of Luis. The spectral wave density plot of buoy 44139 (Fig. 10) does not show the wave containment signature as in Fig. 4 for Bonnie or Danielle. This result illustrates the importance of correctly assessing storm speed and intensity when evaluating TFW potential.

The Holland TFW model values range from 9 to 11 m, located between buoy 44141 and the storm track (Fig. 9), while the other models developed only 8-m waves. These predicted wave heights were 50%–70% of the maximum H_{SIG} reported at buoy 44141. As in Bonnie and Danielle, cross-track TFWs were noted in Luis: the 11–13-m trajectories in the lower-left corner of Fig. 9 directed toward buoy 44142 and the coast of Nova Scotia.

Why the model did not generate sufficiently large TFWs across buoy 44141 was assessed using two special simulations. First, the CHC analysis (Bowyer 2000)

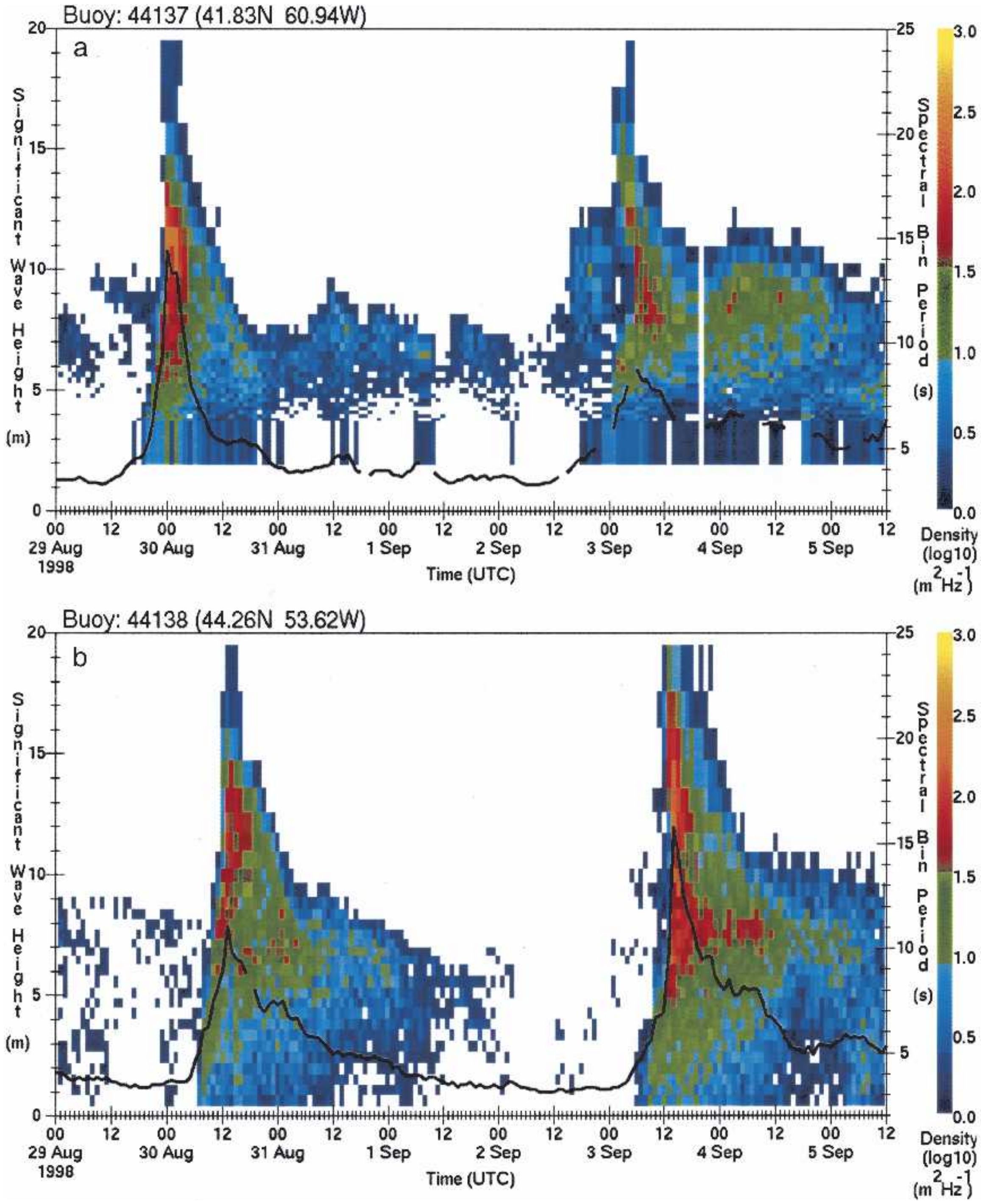

FIG. 4. Plot of measured spectral wave density (m^2 Hz^{-1}) vs data-bin period (s) during Bonnie and Danielle for selected buoys: (a) 44137, (b) 44138, (c) 44141 and (d) 44142. The log10 value of each density bin is color coded according to the scale at extreme right. Superimposed is H_{SIG} (m) reported by the buoy. (Source: Marine and Environmental Data Service: information online at http://www.meds-sdmm.dfo-mpo.gc.ca.)

showed that Luis was much larger than a climatologically sized TC vortex, with a greater radial extent of stronger winds. The model grid domain right of track was increased and the Holland TFW model rerun. Dominant TFWs were farther to the right of track, but only marginally increased in height (circled area around buoy 44141 in Fig. 11a).

Second, the HURDAT dataset for Luis show winds

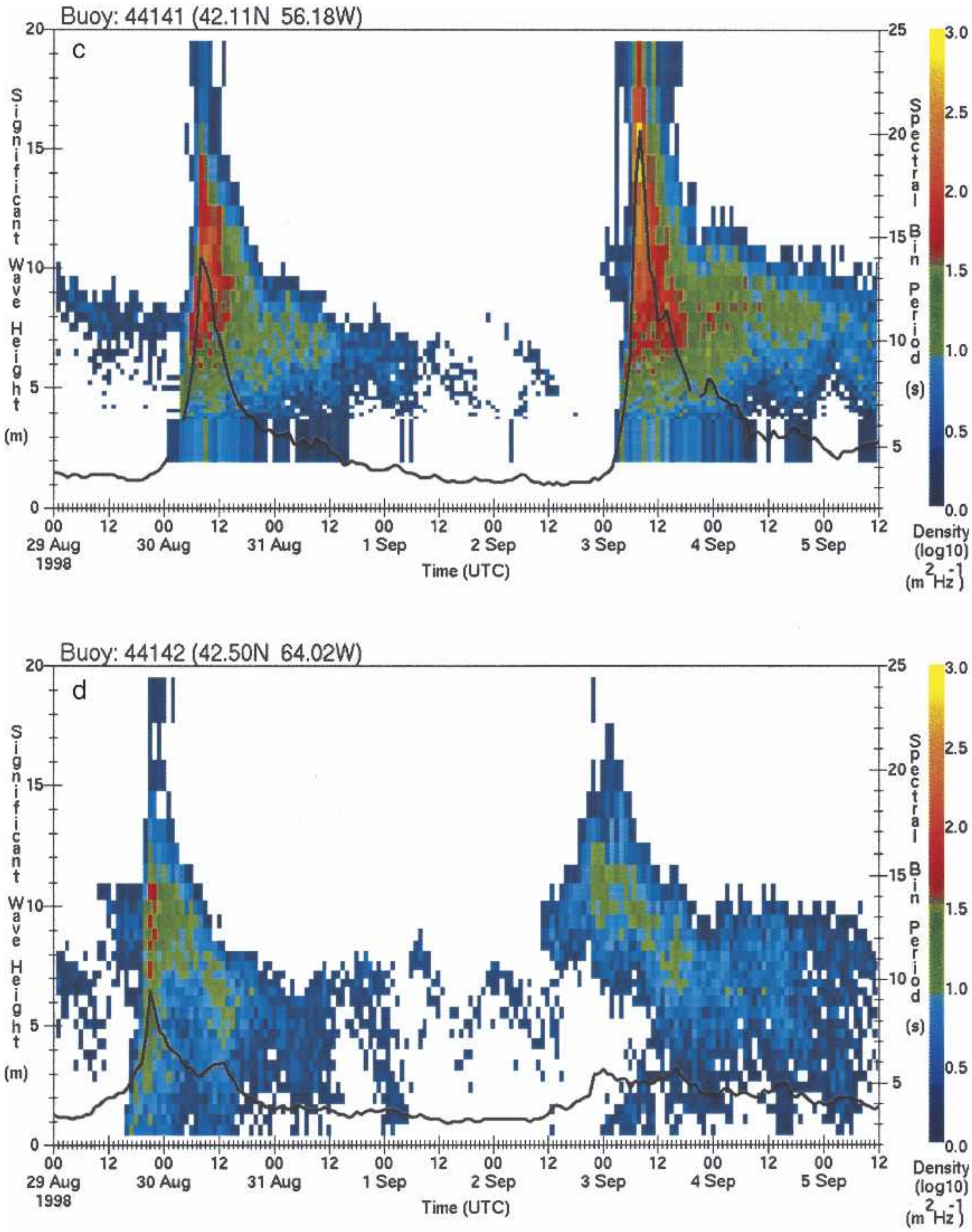

FIG. 4. (*Continued*)

of 51 m s^{-1} (100 kt) before recurvature and 44 m s^{-1} (85 kt) immediately after. Jones et al. (2003) stated that some transitioning TCs do not weaken following recurvature. The *QE II* reported sustained winds near 67 m s^{-1} (130 kt) (Marine Observer 1996) and using a recognized adjustment factor to reduce gusts at higher elevations to a 10-m 1-min wind (Resio et al. 1999) indicates maximum sustained winds of 51 m s^{-1} (100 kt) at the time of Luis's passage through Canadian waters. From Fig. 12 of Bowyer and MacAfee (2005), storms

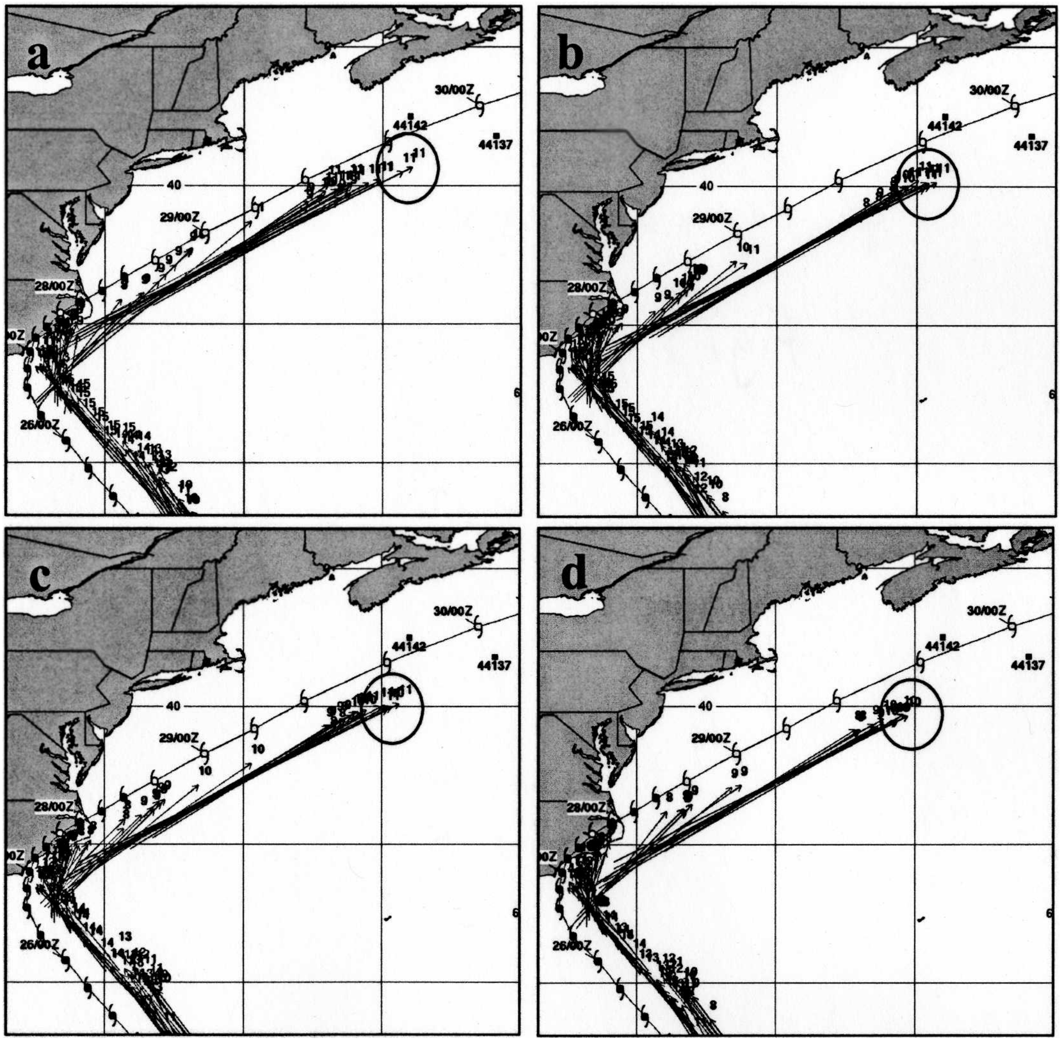

FIG. 5. TFW model results for Bonnie south of Atlantic Canada for an ensemble of parametric wind models: (a) Holland, (b) SLOSH, (c) Vortex, and (d) Rankine. Each model uses a 37 × 25 grid with spacing of 0.1° latitude. Displayed are the dominant TFW trajectories ≥8 m.

moving in excess of 21 m s^{-1} (40 kt) require a wind well in excess of 51 m s^{-1} (100 kt) to develop large TFWs. Luis's speed was over 23 m s^{-1} (45 kt) as it passed buoy 44141, exceeding the optimum speed for TFWs. Hence, the maximum winds after recurvature were manually reanalyzed and the larger-grid Holland TFW model was rerun. The results in Fig. 11b show closer agreement to buoy data (Table 1 and Fig. 10), in both the height and location of the dominant TFW, than did the initial larger grid model run (Fig. 11a). These simulations illustrate the importance of a correct intensity analysis and prediction, and the forecaster's evaluation of storm size in relation to climatological size (for the same intensity) when evaluating the model output.

e. Juan in 2003

On 28–29 September 2003, Juan—a 44 m s^{-1} (85 kt) hurricane—tracked directly over buoy 44142 (Fig. 12) near the arrival of the wave maximum (Table 1). Five hours later the maximum H_{SIG} reached buoy 44258 less than an hour after the nearest approach of Juan. The spectral data with Juan (Fig. 13) show a different signature than in the case of Bonnie and Danielle; increasing wave energy is evident as the storm approached; however, there remained an almost complete lack of long-period swell prior to the storm's arrival. In spite of the larger H_{SIG} at 44142, the spectrum at 44258 shows a more discontinuous spike as the wave energy appears more concentrated than at the offshore buoy.

The largest dominant TFW model trajectory of 18 m (Fig. 12) was directed toward Nova Scotia well east of buoy 44258. These waves originated from the TL grid at 0700 UTC 28 September 2003. Farther to the southwest the 17-m wave directed across the track toward buoy 44258 grew for 19 h from its TL grid at 0600 UTC while the 13-m wave directed toward buoy 44142 grew for

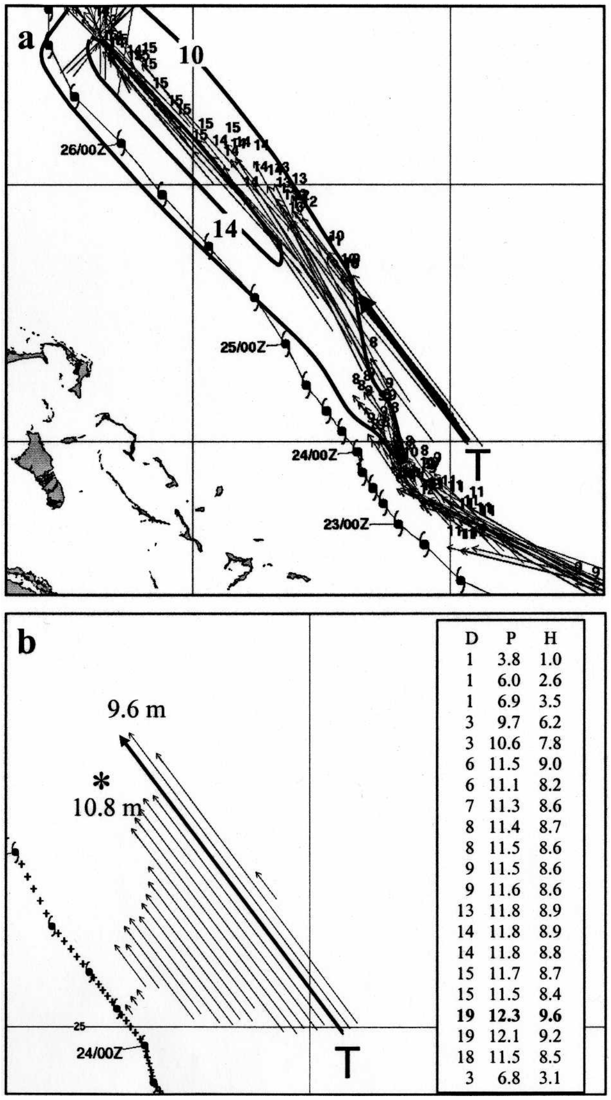

D	P	H
1	3.8	1.0
1	6.0	2.6
1	6.9	3.5
3	9.7	6.2
3	10.6	7.8
6	11.5	9.0
6	11.1	8.2
7	11.3	8.6
8	11.4	8.7
8	11.5	8.6
9	11.5	8.6
9	11.6	8.6
13	11.8	8.9
14	11.8	8.9
14	11.8	8.8
15	11.7	8.7
15	11.5	8.4
19	**12.3**	**9.6**
19	12.1	9.2
18	11.5	8.5
3	6.8	3.1

FIG. 6. Same as in Fig. 5a except for Bonnie approaching the U.S. coast. (a) Zoom of the box in Fig. 3 and (b) detailed model output for all grid calculation rows for initial time 0600 UTC 24 Aug 1998. In both diagrams the dominant TFW trajectory from 0600 UTC 24 Aug 1998 is labeled as T and highlighted by a heavy arrow. The inset table lists the duration D (h), significant wave period P (s), and significant wave height H (m) for each trajectory (in order outward from the track). The asterisk denotes the 2100 UTC 24 Aug 1998 location of a wave maximum of 10.8 m and peak period of 13.0 s as measured by scanning radar altimetry. Heavy black lines are the 10- and 14-m H_{SIG} from Fig. 11b of Moon et al. (2003).

15 h from the 0500 UTC grid (Fig. 14a). During this 2-h period Juan turned northward and accelerated while maintaining the same intensity, highlighting the sensitivity of the TFW model to changes in storm direction and forward speed.

The 10–12-m trajectories in Fig. 14a, ending just north of 40°N, arrived near 1700 UTC 28 September

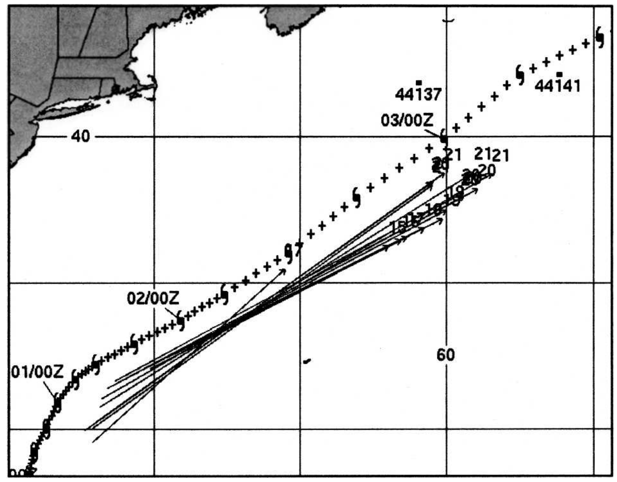

FIG. 7. Same as in Fig. 5a except for Danielle. Displayed are the dominant TFW trajectories ≥15 m north of 30°N.

2003, comparable to the 12-m contour on the National Oceanic and Atmospheric Administration/National Centers for Environmental Prediction Wave Watch III model–North Atlantic Hurricane model (NWW3–NAH) hindcast for 1800 UTC 28 September 2003 (Fig. 14b).

Although the 17-m TFW directed toward buoy 44258 is not the highest, its direction is important because it lines up more directly with the orientation of the Halifax harbor and may account for the public reports of a "wall of water" moving up the harbor, timed with the arrival of the 20 -m H_{MAX} reported at the buoy. Similarly, documented reports of large damaging waves at Peggy's Cove (west of landfall) (CHC; information online at www.ns.ec.gc.ca/weather/hurricane/juan/peggys_cove_e.html) illustrate the importance of monitoring cross-track TFWs in the model output.

Consider the H_{MAX} reported by the buoys (Table 1). Assuming that the wind wave generating conditions in Juan were constant, Lopatoukhin et al. (2000) showed that the wind waves obey a Rayleigh distribution. Obtaining an estimate of the ratio H_{MAX}:H_{SIG} from this distribution and applying Forristall's correction factor of 0.907, as suggested by Lopatoukhin et al. (2000), yields an average H_{MAX}:H_{SIG} ratio of 1.85 (based on 15–18 h of wave growth and a T_{SIG} of 15 s). However, H_{MAX}:H_{SIG} exceeded 2.0 at both buoys. This ratio may be real and explained by the vagaries of wave spectra. It could also be argued that, because the H_{MAX} is the largest measured wave in the preceding hour and the H_{SIG} is a statistical rendering of the spectral data over a 40-min period ending at the data collection hour (AXYS 1996), the largest H_{SIG} actually arrived before the reported H_{SIG}, more in conjunction with the timing of the H_{MAX} in the early part of the hour. While it is inappropriate to work backward from the H_{MAX} to ob-

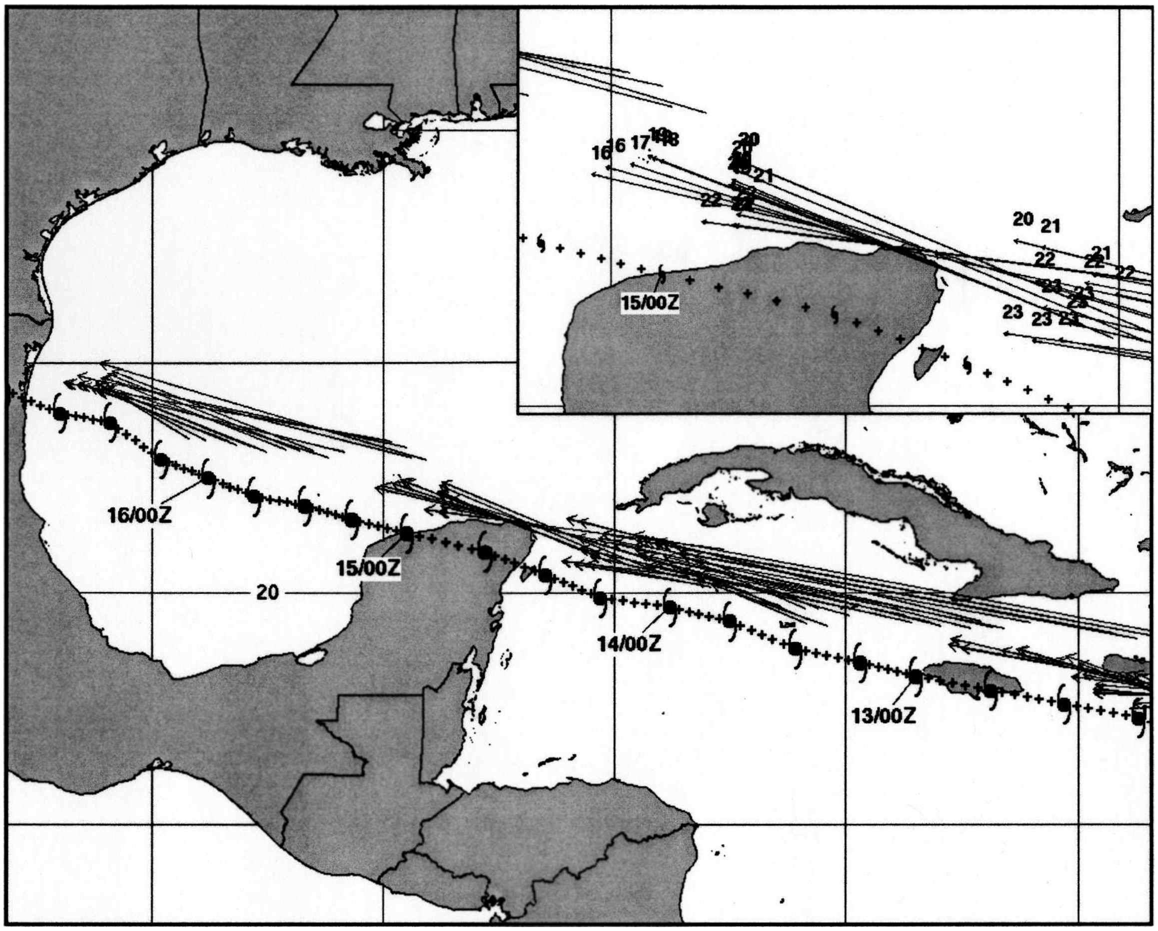

FIG. 8. Same as in Fig. 5a except for Gilbert. Displayed are dominant TFW trajectories ≥15 m north of 10°N. The inset zooms into the cluster of trajectories passing north of the Yucatan Peninsula.

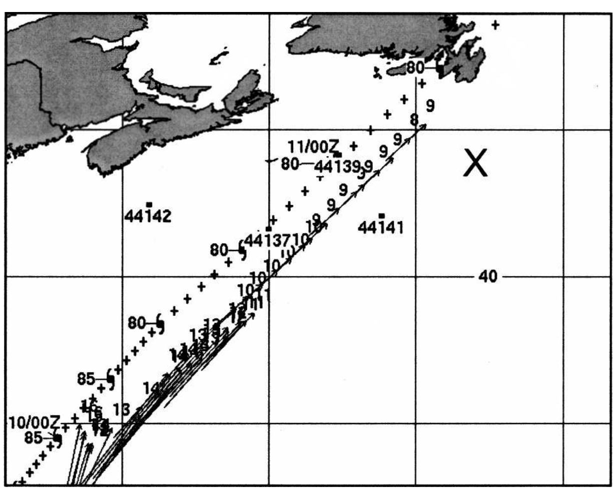

FIG. 9. Same as in Fig. 5a except for Luis. The **X** denotes the QE II position at 0430 UTC 11 Sep 1995. Displayed are the dominant TFW trajectories ≥8 m north of 30°N.

tain a new H_{SIG}, we speculate that the waves may not have been accurately represented by the reported H_{SIG}.

f. Gulf of Mexico

The ability of the TFW model to depict wave development in non-trapped-fetch situations and in regions other than midlatitudes is illustrated by five tropical cyclones in the Gulf of Mexico: Earl (in 1998), Bret (in 1999), Helene (in 2000), Lili (in 2002), and Isidore (in 2002). These examples were selected only because their track was near or left of a buoy with available spectral data. Figure 15 shows the track of each TC, dominant TFW trajectories (Holland model), and spectral wave density and H_{SIG} buoy data. The TFW model is a deep-water model. Accordingly, the shallow depth of the Gulf of Mexico and the wide coastal zone must be considered in assessing the model output.

In Fig. 15a, the TFW model depiction of Earl builds waves to 13 m after crossing buoy 42039, which

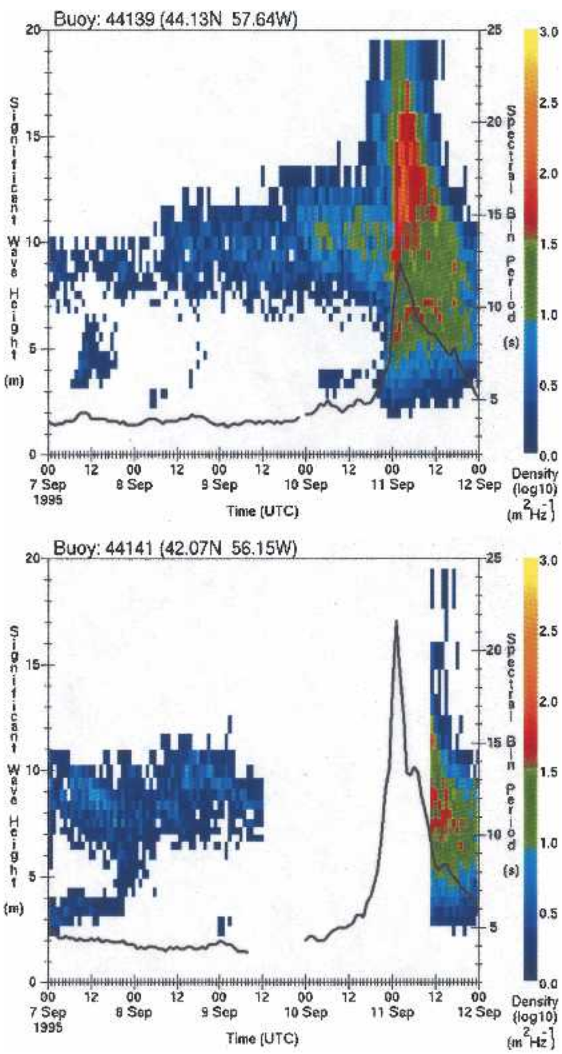

FIG. 10. Same as in Fig. 4 except for Luis.

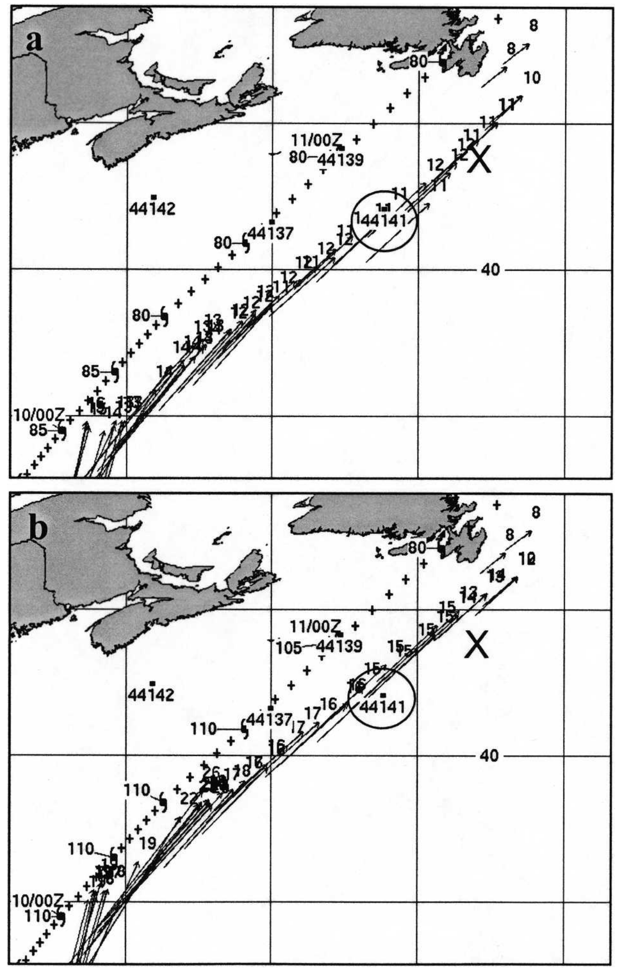

FIG. 11. Same as in Fig. 9 except using a larger model grid (51 × 41) and different track location maximum winds: (a) HURDAT and (b) CHC reanalysis.

reported a maximum H_{SIG} of 10 m. The full set of trajectories for the grid at 0600 UTC 2 September (not shown) gave waves of 10–12 m that grew for 19 h, arriving at buoy 42039 at 0100 UTC 3 September.

In Fig. 15b, the TFW model depiction of Bret (in 1999) shows dominant waves of 11–13 m north of buoy 42020, which reported a maximum H_{SIG} of 8 m. The full set of trajectories for the grid at 1200 UTC 22 August (not shown) gave waves of 4–9 m that grew for 5 h before arriving at buoy 42020 near the reported maximum H_{SIG}.

In Fig. 15c, the TFW model depiction of Lili shows dominant waves of 20 m near buoy 42041, which reported a maximum H_{SIG} over 10 m (missing data at the peak). These trajectories originated from a shallow water area near 23.5°N, 83.5°W. Hence, the number of hours of growth and wave height are overforecast. This example illustrates that TFW model output must be carefully evaluated using knowledge of the model limitations and local bathymetry.

In Fig. 15d, the TFW model depiction of Helene shows dominant waves of 2–3 m near buoy 42003 (maximum H_{SIG} of 3 m) and northward trajectories growing to 8 m after crossing buoy 42039 (maximum H_{SIG} of 4 m). Note the 6-m trajectories ending southwest of 42039. These trajectories began at 2300 UTC 20 September (not shown) and grew for 23 h arriving near the peak in the H_{SIG} of buoy 42039. Detailed trajectories from the grid at 1700 UTC 20 September arrive at buoy 42003 20 h later with a height of 3 m. This example illustrates that trajectories and their duration from each row of a specific hourly grid provide important details that may not be obvious when examining only the dominant TFW trajectories.

In Fig. 15e, the TFW model depiction of Isidore shows dominant waves of 7 m east of buoy 42001, which reported a maximum H_{SIG} near 6 m for 8 h beginning 0500 UTC 25 September. Similarly, buoy 42041 reported over 6 m for 16 h beginning at 0500 UTC 25 September. Several consecutive hourly grids (not shown) generated waves of 6 m with duration lead-

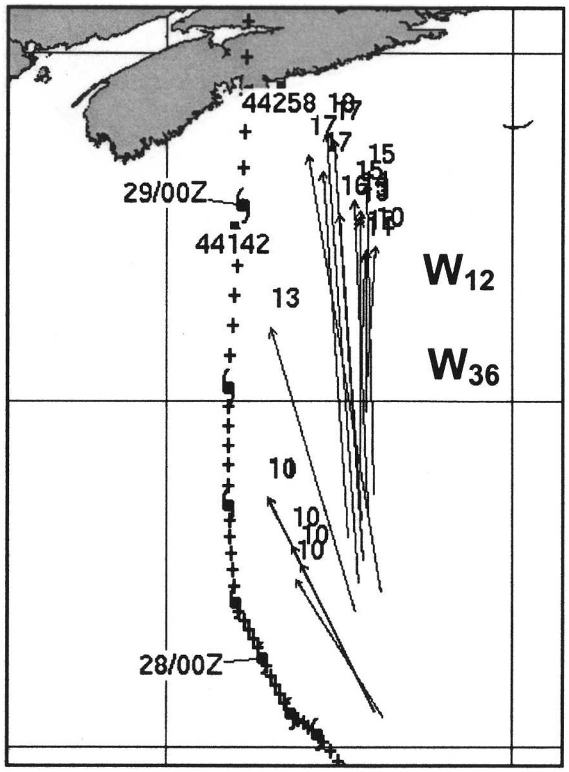

FIG. 12. Same as in Fig. 5a except for Juan: dominant TFW trajectories ≥10 m north of 30°N with the highest value of 18 m right of track. The label W_{36} denotes the position of the 36-h CMC WAM forecast maximum in the H_{SIG} field of 6 m valid at 0000 UTC 29 Sep 2003; the label W_{12} is the 12-h CMC WAM forecast of 5 m valid at the same time.

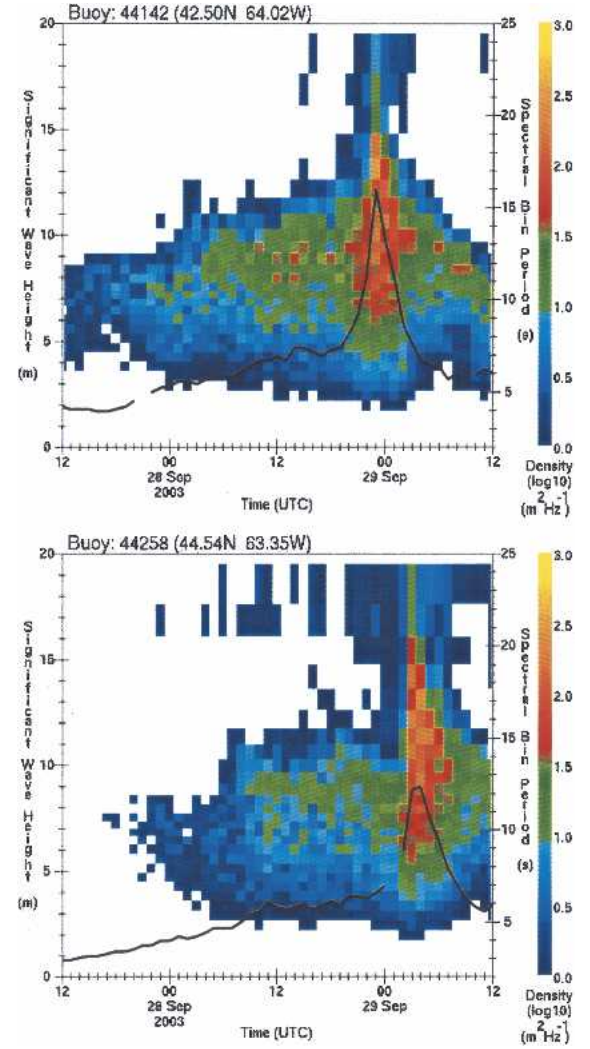

FIG. 13. Same as in Fig. 4 except for Juan.

ing to arrival near 42041 near the end of their growth period.

5. Operational utility

The CHC has used various versions of the TFW model operationally since 2000 (MacAfee and Peters 1999; MacAfee and Bowyer 2000b). A single model (similar to the Holland TFW model) used during the 2003 hurricane season allowed CHC forecasters to provide quality wave guidance to regional Environment Canada weather centers. This was critical in that the Canadian Meteorological Centre's (CMC) wave model (WAM) (WAMDI Group 1988) was of little value due to the poor performance of its atmospheric model [the Global Environmental Multiscale (GEM) model; Côté et al. 1998] in handling a number of the tropical systems and, in particular, Juan. The 36-h WAM forecast valid for 0000 UTC 29 September 2003 was 6 m, located 444 km (240 n mi) southeast of the coast of Nova Scotia (Fig. 12). Based on CHC TFW model guidance, the Maritimes Weather Centre (MWC) issued the official forecast as 12 m, just south of Nova Scotia. Twenty-four hours later, the 12-h forecasts for 0000 UTC 29 September 2003 were 5 m and 14 m for the WAM and MWC, respectively (Fig. 12).

Note that the hurricane version of the NWW3–NAH (Tolman 2002; Tolman et al. 2002) is expected to capture TFW situations more frequently than the CMC WAM because the NWW3-NAH has a wind field generated by the Geophysical Fluid Dynamics Laboratory (GFDL) hurricane wind model. Hence, the role of the TFW model is to focus attention on a particular portion of the wave field by allowing the forecaster to generate track prediction scenarios and assess the impact of the generated TFWs. This is especially useful in the interval between operational runs of spectral wave models.

The CHC Hurricane Information Statement (WTCN31 CWHX) issued at 0000 UTC 4 September 2003 for Hurricane Fabian stated, "CHC trapped-fetch wave model indicates very high wave heights to the east side of Fabian . . . especially as it moves through Grand Banks of Newfoundland on Sunday. WW3 model con-

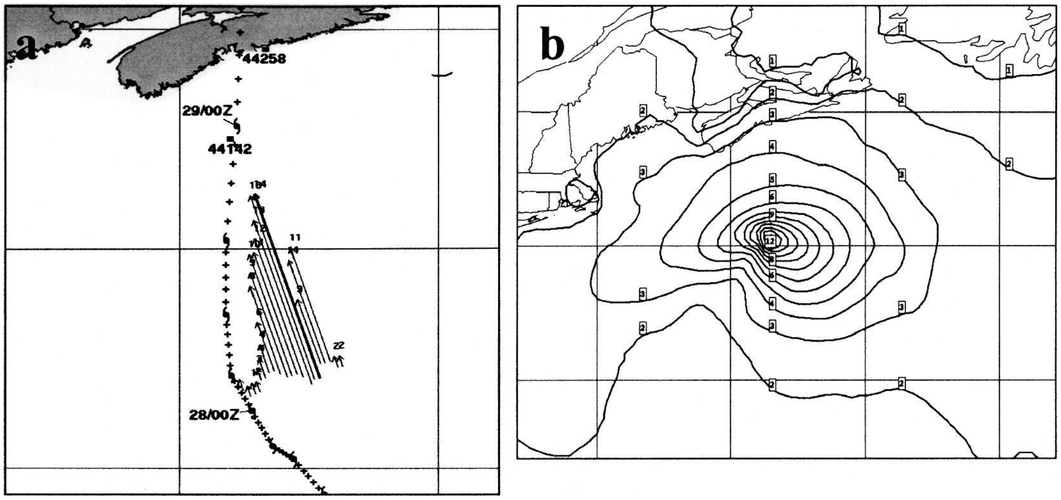

FIG. 14. (a) Detailed model output for Juan for all grid calculation rows for initial time 0500 UTC 28 Sep 2003 with end points north of 40°N arriving from 1700 to 2200 UTC 28 Sep 2003. (b) WW3 hurricane model hindcast for 1800 UTC 28 Sep 2003 (Source: Marine Modeling and Analysis Branch: information online at ftp://polar.ncep.noaa.gov/pub/history/waves/.)

curs with sig wave heights in excess of 15 m." Figure 16 shows the Holland TFW model output for Fabian with phenomenally large H_{SIG} of 18–24 m. The most advanced and highest waves were generated from the hourly grid at 1200 UTC 6 September 2003 growing for 35 h (Figs. 17b and 17c). For comparison, the 36-h WAM forecast H_{SIG} maximum, valid at 0000 UTC 8 September 2003, was 5 m (labeled W_{36} in Fig. 16) and the NWW3–NAH hindcast showed a 10-m contour near the location of the wave arrival (Figs. 17a and 17b). From an understanding of TFW theory (Bowyer and MacAfee 2005) and this model output, it is hypothesized that Fabian's combination of wind strength and gradual acceleration make it a case of extreme wave containment. However, Bowyer and MacAfee (2005) outlined the limitations of the significant wave method and Bretschneider equations and that an overforecast of wave heights in situations of extreme wave containment is likely. There were no corroborating data with this storm since it remained outside the buoy network. However, the vessel *Pacific Attitude* sank with the loss of three lives. The location of the *Pacific Attitude* at the time it signaled distress (2130 UTC 7 September 2003) is indicated by a **P** in Fig. 16.

These two examples demonstrate the most important application of the TFW model: its utility as an operational tool for making quick decisions on the size, location, and arrival time of the largest TFWs associated with TCs. Spectral wave models (e.g., NWW3–NAH) should give comparable results and a more complete picture of the wave field, if provided with the proper storm data. However, when the data change, there is insufficient time for additional full spectral wave model runs. Conversely, the TFW model can be rerun at forecasters' discretion to provide guidance while waiting for the next full spectral wave model run.

The use of different wind models, as demonstrated here, may provide a measure of forecaster confidence in the solutions. For example, strong consensus between the models may indicate that the storm parameters are not near critical thresholds since minor perturbations in these parameters can result in vastly different TFWs (Bowyer and MacAfee 2005). Even within a single model, a cluster of trajectories indicates consistent wave development from successive initial wave point sets. Conversely, a single trajectory emerging from a cluster may be an indication of a threshold being attained within a narrow region of the storm and notifies the forecaster of potentially larger waves than might otherwise be expected.

6. Summary and conclusions

Very high waves have been recorded in Canadian waters with the passage of tropical cyclones (TCs) (MacAfee and Bowyer 2000a). An investigation of these waves led to the development of a Lagrangian-based trapped-fetch wave (TFW) model, driven by a high-resolution [11 km (6 n mi)] storm-relative parametric hurricane wind model. The TFW model was validated against buoy and U.S. scanning radar altimetry data and compared against full spectral wave model output. Case studies were used to assess the sensitivity of the TFW model to the input wind field to provide a deeper understanding of the TFW phenomenon and to highlight the utility of the model.

Case studies of Bonnie, Danielle, Luis, and Juan, as well as examples in the Gulf of Mexico, were presented. In most cases the TFW model performed well, gener-

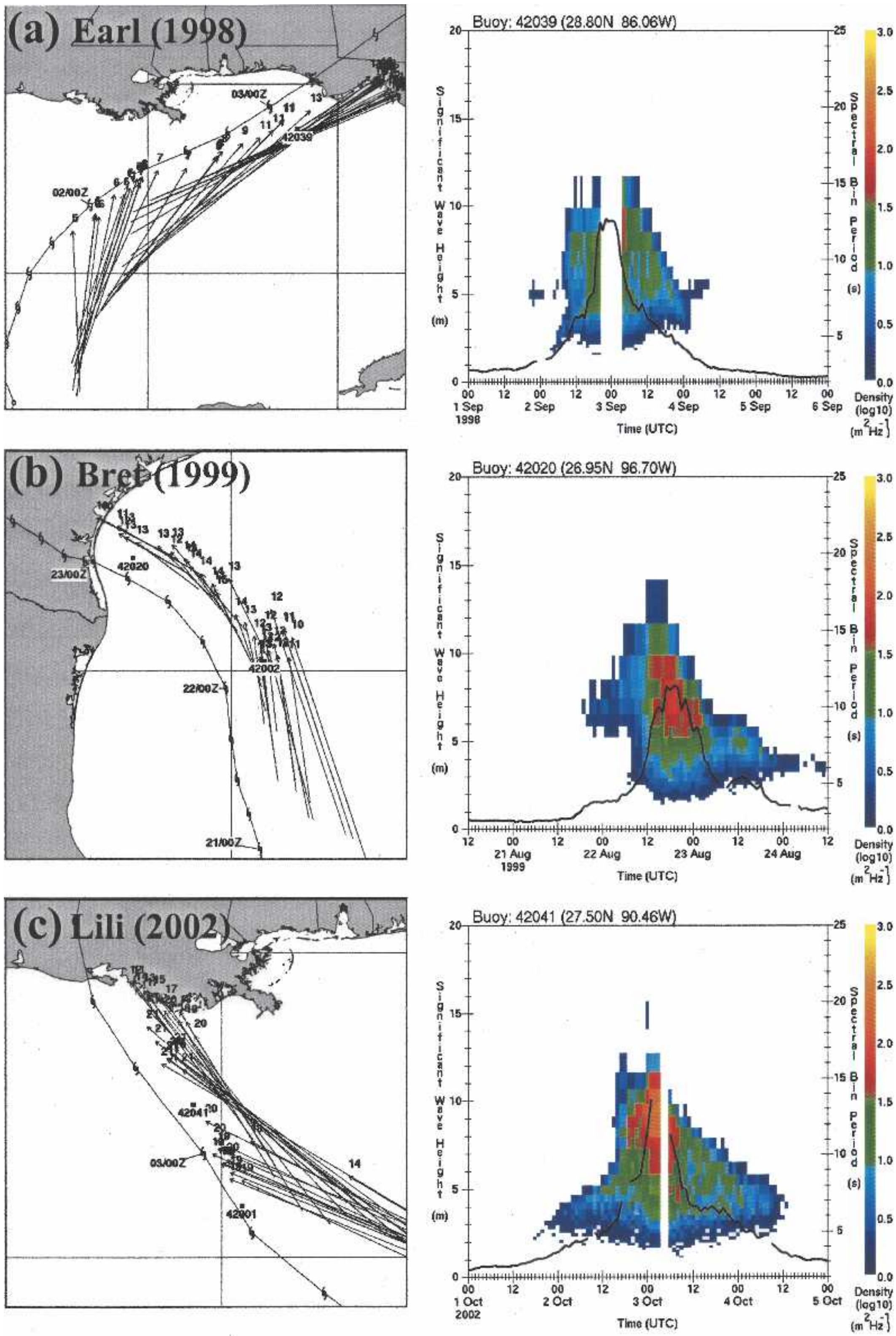

FIG. 15. TFW model output of dominant trajectories for storms passing near buoys in the Gulf of Mexico: (a) Earl ≥5 m, (b) Bret ≥10 m, (c) Lili ≥10 m, (d) Helene ≥1 m, and (e) Isidore ≥5 m. (Source: National Data Buoy Center: information online at http://www.ndbc.noaa.gov/historical_data.shtml.)

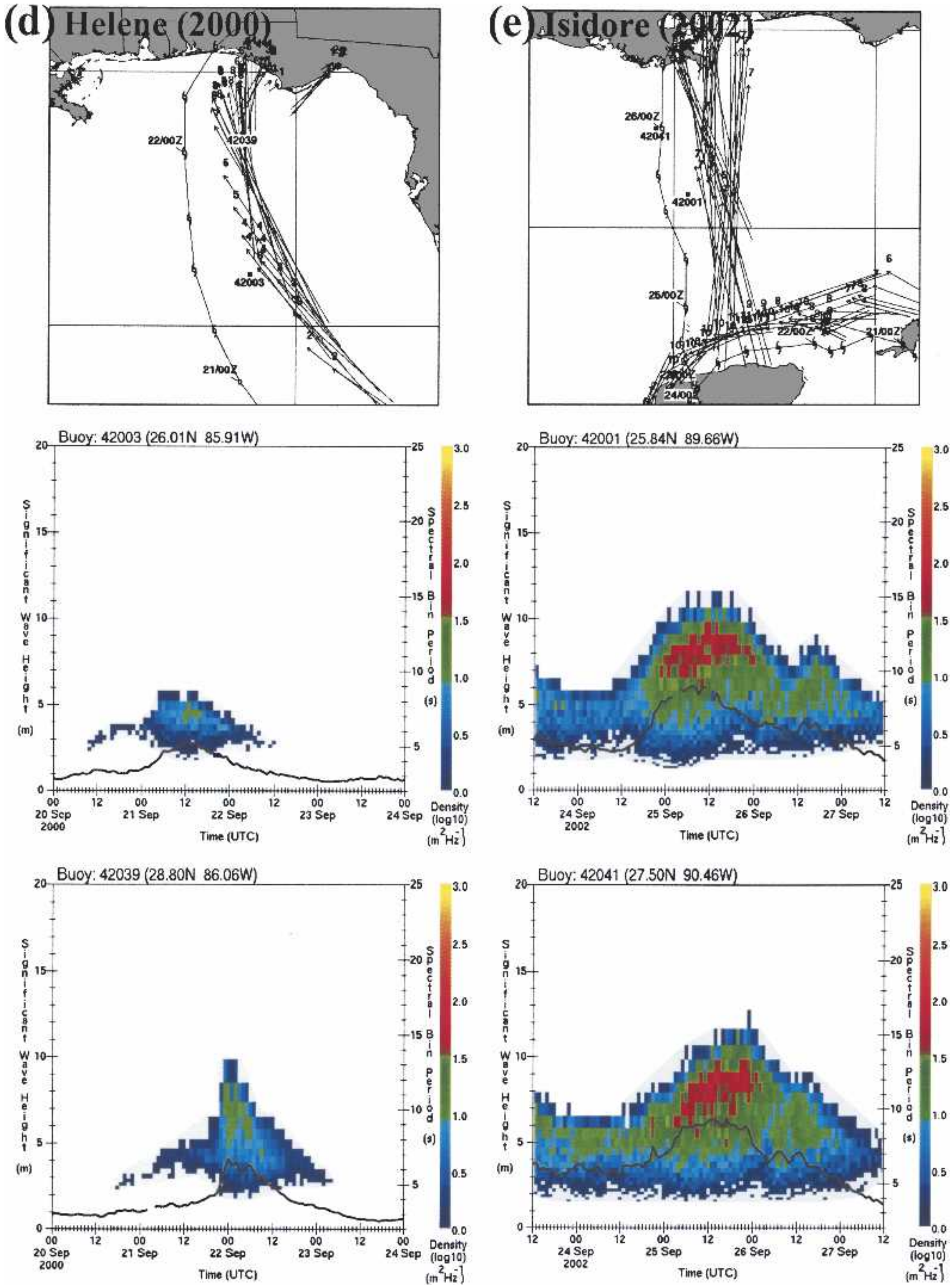

FIG. 15. (*Continued*)

ating wave heights comparable to observations. Luis was problematic in that its size exceeded that of a typical TC and uncertainty remains as to the intensity following recurvature. A TFW model run using a reanalysis of Luis's intensity and an expanded model domain produced model results more consistent with the observations, illustrating the sensitivity of the TFW model to the underlying wind field distribution. Further sensitivity tests consisted of an intercomparison of TFWs generated by using an ensemble of four parametric hurri-

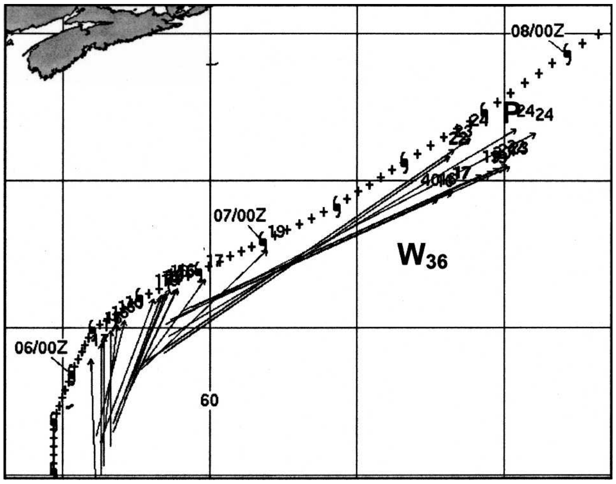

FIG. 16. Same as in Fig. 5a except for Fabian. Displayed are the dominant TFW trajectories ≥15 m north of 30°N with the highest TFW of 24 m. The **P** denotes the location (42°15′N, 49°58′W) of the *Pacific Attitude* when it signaled distress at 2130 UTC 7 Sep 2003. The W_{36} denotes the 36-h CMC WAM forecast maximum in the H_{SIG} field of 5 m valid at 0000 UTC 8 Sep 2003.

cane wind models. The degree of similarity between model TFW heights and duration provided insight into the degree of wave containment.

Bonnie, Danielle, and Juan were storms exhibiting strong wave containment as seen by the proximity of the wave maximum to the storm center and by the steepness of the horizontal gradient in the wave height field at the buoys. The importance of storm wave containment was illustrated by the similarity in TFWs with (a) Bonnie, a slow-moving hurricane versus an accelerating tropical storm following recurvature, and (b) Danielle, an accelerating Saffir–Simpson category-1 hurricane versus Gilbert, a slow-moving category-5 hurricane.

In most TCs, the dominant waves move parallel to the storm (Bowyer and MacAfee 2005); however, several instances of significant cross-track TFWs were noted. In particular, during Juan, cross-track TFWs were predicted at the coast near or west of landfall and later documented in coastal damage reports, highlighting the need for scrutiny of all TFW trajectories along the storm track.

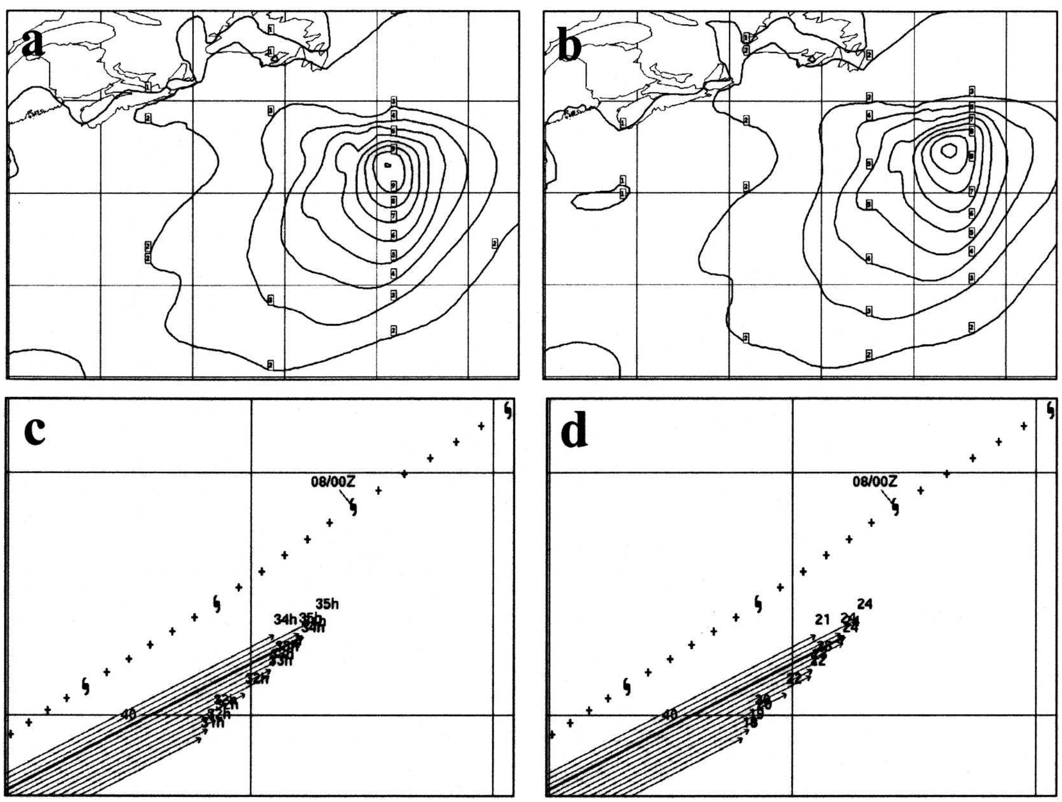

FIG. 17. Comparison of WW3 (hurricane) hindcasts and maximum TFW trajectories for Fabian: (a), (b) WW3 at 2100 UTC 7 Sep 2003 and 0000 UTC 8 Sep 2003 and (c), (d) duration and H_{SIG} of the dominant TFW trajectories from the grid at 1200 UTC 6 Sep 2003.

The advantages of the TFW model presented in this paper are operational speed, the ability for forecaster intervention with last-minute changes in track and intensity, and high quality predictions of trapped-fetch waves. Finally, as suggested by the case study of Luis, the TFW model may be an effective tool for qualifying the HURDAT archival data where robust wave data exist. Future work will include reexamining the cases presented in this paper using other wave growth formulations, refining the TFW calculation method to include fetch width limitations, coastal zone adjustments, grid domain as a function of storm size, and a rigorous statistical validation against observations and spectral wave model output.

Acknowledgments. The authors would like to acknowledge HRD and Mark Powell for providing FTP access to the H*WIND analysis, Doug Mercer for pointing us in the direction of key papers and buoy spectral data, Garry Pearson and Serge Desjardins for their critical review of this paper, the *Weather and Forecasting* editor and reviewers for their numerous excellent suggestions and corrections, and Angie Ward-Smith and Dawn Taylor-Prime for their resourcefulness in locating references.

REFERENCES

AXYS, 1996: Meteorological and oceanographic measurements from Canadian weather buoys: A review of sensors, data reduction, transmission, quality control and archival methods. AXYS Environmental Consulting Rep. SP-70, 57 pp.

Bowyer, P. J., 2000: Phenomenal waves with a transitioning tropical cyclone (Luis, the Queen, and the buoys). Preprints, *24th Conf. on Hurricanes and Tropical Meteorology*, Fort Lauderdale, FL, Amer. Meteor. Soc., 294–295.

——, and A. W. MacAfee, 2005: The theory of trapped-fetch waves with tropical cyclones—An operational perspective. *Wea. Forecasting,* **20,** 229–244.

Bretschneider, C. L., and E. E. Tamaye, 1976: Hurricane wind and wave forecasting techniques. Preprints, *15th Conf. on Coastal Engineering,* Vol. 1, Honolulu, HI, Amer. Soc. Civil Eng., 202–237.

Côté, J., S. Gravel, A. Méthot, A. Patoine, M. Roch, and A. Staniforth, 1998: The operational CMC–MRB multiscale (GEM) model. Part I: Design considerations and formulation. *Mon. Wea. Rev.,* **126,** 1373–1395.

DeMaria, M., S. Aberson, K. V. Ooyama, and S. J. Lord, 1992: A nested spectral model for hurricane track forecasting. *Mon. Wea. Rev.,* **120,** 1628–1643.

Franklin, J. L., B. L. Black, and K. Valde, 2003: GPS dropwindsonde wind profiles in hurricanes and their operational implications. *Wea. Forecasting,* **18,** 32–44.

Holland, G. J., 1980: An analytic model of the wind and pressure profiles in hurricanes. *Mon. Wea. Rev.,* **108,** 1212–1218.

Houston, S. H., and M. D. Powell, 1994: Observed and modeled wind and water-level response from Tropical Storm Marco (1990). *Wea. Forecasting,* **9,** 427–439.

——, W. A. Shaffer, M. D. Powell, and J. Chen, 1999: Comparisons of HRD and SLOSH surface wind fields in hurricanes: Implications for storm surge modeling. *Wea. Forecasting,* **14,** 671–686.

Jones, S. C., and Coauthors, 2003: The extratropical transition of tropical cyclones: Forecast challenges, current understanding, and future directions. *Wea. Forecasting,* **18,** 1052–1092.

Krayer, W. R., and R. D. Marshall, 1992: Gust factors applied to hurricane winds. *Bull. Amer. Meteor. Soc.,* **73,** 613–617.

Lopatoukhin, L. J., V. A. Rozhkov, V. E. Ryabinin, V. R. Swail, A. V. Boukhanovsky, and A. B. Degtyarev, 2000: Estimation of extreme wind wave heights. JCOMM Tech. Rep. 9, Joint WMO/IOC Technical Commission for Oceanography and Marine Meteorology, 70 pp.

MacAfee, A. W., and B. Peters, 1999: Canadian Hurricane Centre operational analytical wind model. Preprints, *23d Conf. on Hurricanes and Tropical Meteorology,* Dallas, TX, Amer. Meteor. Soc., 889–892.

——, and P. J. Bowyer, 2000a: Trapped-fetch waves in a transitioning tropical cyclone (Part I—The need and the theory). Preprints, *24th Conf. on Hurricanes and Tropical Meteorology*, Fort Lauderdale, FL, Amer. Meteor. Soc., 292–293.

——, and P. J. Bowyer, 2000b: Trapped-fetch waves in a transitioning tropical cyclone (Part II—Analytical and predictive model). Preprints, *24th Conf. on Hurricanes and Tropical Meteorology*, Fort Lauderdale, FL, Amer. Meteor. Soc., 165–166.

Marine Observer, 1996: Hurricane 'Luis,' the Queen Elizabeth 2, and a rogue wave. *Mar. Observer,* **66** (333), 134–137.

Moon, I. L., I. Ginis, T. Hara, H. L. Tolman, C. W. Wright, and E. J. Walsh, 2003: Numerical simulation of sea surface directional wave spectra under hurricane wind forcing. *J. Phys. Oceanogr.,* **33,** 1680–1706.

Phadke, A. C., C. D. Martino, K. F. Cheung, and S. H. Houston, 2003: Modeling of tropical cyclone winds and waves for emergency management. *Ocean. Eng.,* **30,** 553–578.

Resio, D. T., V. R. Swail, R. E. Jensen, and V. J. Cardone, 1999: Wind speed scaling in fully developed seas. *J. Phys. Oceanogr.,* **29,** 1801–1811.

Saville, T., 1954: The effect of fetch width on wave generation. U.S. Army Coastal Engineering Research Center Tech. Memo. 70, 10 pp.

Tolman, H. L., 2002: Validation of WAVEWATCH III version 1.15 for a global domain. NOAA/NWS/NCEP/OMB Tech. Note 213, 33 pp. [Available online at http://polar.ncep.noaa.gov/waves/wavewatch.]

——, B. Balasubramaniyan, L. D. Burroughs, D. V. Chalikov, Y. Y. Chao, H. S. Chen, and V. M. Gerald, 2002: Development and implementation of wind-generated ocean surface wave models at NCEP. *Wea. Forecasting,* **17,** 311–333.

Vickery, P. J., P. F. Skerlj, and L. A. Twisdale, 2000: Simulation of hurricane risk in the U.S. using empirical track model. *J. Struct. Eng. Amer. Soc. Civil Eng.,* **126**, 1222–1237.

WAMDI Group, 1988: The WAM model—A third-generation ocean wave prediction model. *J. Phys. Oceanogr.,* **18,** 1775–1810.

WMO, 1998: *Guide to Wave Analysis and Forecasting.* 2d ed. WMO-No. 702, 159 pp.

Wright, C. W., and Coauthors, 2001: Hurricane directional wave spectrum spatial variation in the open ocean. *J. Phys. Oceanogr.,* **31,** 2472–2488.